Efficient Solar-Driven Nitrogen Fixation over Carbon–Tungstic-Acid Hybrids

Xiaoman Li, Wenzhong Wang,* Dong Jiang, Songmei Sun, Ling Zhang, and Xiang Sun[a]

Abstract: Ammonia synthesis under mild conditions is of supreme interest. Photocatalytic nitrogen fixation with water at room temperature and atmospheric pressure is an intriguing strategy. However, the efficiency of this method has been far from satisfied for industrialization, mainly due to the sluggish cleavage of the N N bond. Herein, we report a carbon–tungstic-acid ($WO_3 \cdot H_2O$) hybrid for the co-optimization of N_2 activation as well as subsequent photoinduced protonation. Efficient ammonia evolution reached 205 mmol $g^{@1}$ $h^{@1}$ over this hybrid under simulated sunlight. Nitrogen temperature-programmed desorption revealed the decisive role of carbon in N_2 adsorption. Photoactive $WO_3 \cdot H_2O$ guaranteed the supply of electrons and protons for subsequent protonation. The universality of carbon modification for enhancing the N_2 reduction was further verified over various photocatalysts, shedding light on future materials design for ideal solar energy utilization.

Artificial ammonia (NH_3) synthesis by the reduction of atmospheric nitrogen is of great importance for the human society.[1] The industrial Haber–Bosch process for NH_3 production using N_2 and H_2 is generally conducted under severe conditions (300–450 8C, 15–25 MPa) over iron-based catalysts, accompa-nied with massive energy consumption as well as fossil-derived CO_2 emission.[1c, 2] An energy-efficient and environmentally friendly NH_3 synthesis is therefore highly desirable. Solar-driven N_2 reduction by water using semiconductor photocatalysis at room temperature and atmospheric pressure has been one promising strategy.[3] These photocatalysts, however, still suffer from low quantum efficiencies, even in the presence of various hole-scavengers or cocatalysts. The inefficient NH_3 evolution is mainly attributed to the sluggish N_2 activation on the semiconductor surface that together with subsequent photoinduced protonation, contributes to the elementary steps of the whole photocatalytic process.

[a] X. Li, Prof. W. Wang, D. Jiang, S. Sun, L. Zhang,
X. Sun Shanghai Institute of Ceramics
Chinese Academy of Sciences
Shanghai 200050 (P. R. China)
E-mail: wzwang@mail.sic.ac.cn

Actually, sufficient N_2 activation is the prerequisite of its reduction during various processes. In the biogeochemical N_2 cycle, a molybdenum–iron (MoFe)-containing protein within the nitrogenase activates N_2 molecules using a core MoFe co-factor.[4] In classical Haber–Bosch reactions, Fe or Ru-based cat-alysts provide the active sites for N_2 activation.[5] For photoca-talysis, some studies learned from above cases and tried to find the answer in structures containing metallic active centers such as the iron-doped TiO_2 reported by Schrauzer et al. and the FeMoS-chalcogels core cluster reported by Banerjee et al.[3c, 6] Besides this, researchers also explored the feasibility of nonmetallic centers for N_2 activation. Recently, efficient N_2 photoreduction to NH_3 has been achieved over BiOBr nano-sheets and graphitic carbon nitride (g-C_3N_4) under visible-light irradiation, benefiting from enhanced N_2 activation at the O and N vacancies, respectively.[7]

In addition to N_2 pre-activation on catalyst surface, subse-quent photoinduced protonation is another key point. For in-stance, the electron-donating iron protein within nitrogenase plays an indispensable role in N_2 reduction. As an n-type semi-conductor with widespread elements, tungsten oxide hydrates have attracted much attention in energy storage and photoca-talysis.[8] Due to the outstanding electron and proton conduc-tivity, herein $WO_3 \cdot H_2O$ was selected as the photoactive material to explore the N_2 photofixation. Greatly enhanced N_2 reduction to ammonia (205 mmol $g^{@1}$ $h^{@1}$) was achieved by carbon modifi-cation under simulated sunlight irradiation. Careful studies evi-dently revealed the indispensable roles of carbon in surface N_2 dissociation and $WO_3 \cdot H_2O$ in photoinduced protonation, re-spectively. Furthermore, the carbon modification strategy was found universal for enhancing photocatalytic ammonia evolu-tion over other semiconductor materials.

For the first time, pristine tungstic acid (HWO-p) was synthe-sized using a microwave-assisted method. Surface decoration of carbon (HWO/C) was achieved by a post-microwave treat-ment of HWO-p in a PEG-200/water mixed solution with differ-ent amount of glucose (mg, for further details, see the Sup-porting Information), namely, HWO/C-X (X, 0–1000). For refer-ence, HWO-p was treated under identical conditions without the addition of glucose (HWO). As indicated by the XRD pat-terns (Supporting Information, Figure S1), the post-microwave exposed (120) facets of HWO and HWO/C by the etching of the PEG and carbon modification did not change the crystal-line structure of the pristine $WO_3 \cdot H_2O$. As shown in the TEM and SEM images (Figure 1, Supporting Information, Figure S2), as-prepared HWO-p presents as microspheres with a hierarchi-cal structure composed of 2D sheet-like building blocks, and
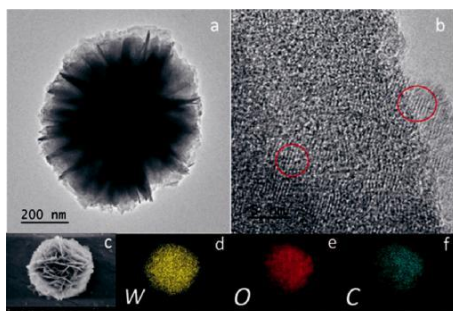
Figure 1. (a, b) TEM image and HRTEM image of HWO/C. (c) SEM image of HWO/C. (d–f) EDS mapping of O, W and C of (c), respectively.

surface decoration of carbon does not change the morpholo-gy. The HRTEM (Figure 1 b) image shows that the carbon coat-ing on the HWO layer and the carbon is partly amorphous. The interlayer spacing in the crystallized carbon, around 3.4 Å, cor-responds to the 002 distance of graphitic carbon. Meanwhile, energy-dispersive X-ray spectroscopy (EDS) mapping (Fig-ure 1 d–f) evidently confirmed the uniform fold of carbon layers on the HWO base material. The successful decoration of carbon on $WO_3 \cdot H_2O$ surface can also be traced by the diffuse reflectance spectra (DRS) (Supporting Information, Figure S3). As shown in Figure S3 (Supporting Information), the HWO/C-X samples present gradually increased light absorption in the near-infrared region with the increase of glucose addition. The actual loading amounts of carbon in HWO/C@X samples were roughly estimated by thermogravimetric analysis (Supporting Information, Figures S4 and S5).

Photocatalytic N_2 fixation over various materials was ex-plored using water as the reactant in the absence of any or-ganic scavengers or metal cocatalysts. As shown in Figure 2 a, after 1 h of Xe lamp irradiation, only low levels of NH_3 evolu-tion (3.8 mmol g^{-1} h^{-1}) were detected using HWO. However, the NH_3 production was greatly enhanced by surface carbon deco-ration. In Figure 2 b, with the increase of carbon decoration, the NH_3 evolution over HWO/C-X samples presented a mono-tonic increase with the increase of X, reaching about 220 mmol g^{-1} h^{-1} over HWO/C1000, a 58-fold increase com-pared to pure HWO. According to thermogravimetric analysis, the unobvious enhancement from HWO/C0 to HWO/C1000 can be attributed to the saturation of carbon layer decoration on the HWO surface, which can also be reflected by the DRS data (Supporting Information, Figure S6). Herein, HWO/C500 is selected for further discussion. As shown in Figure 2 c, the NH_3 production increased linearly, reaching 205 mmol g^{-1} h^{-1} after 60 min irradiation. The system did not evolve NH_3 in the ab-sence of light irradiation or nitrogen atmosphere. The NH_3 pro-duction under visible-light irradiation was 31 % of that under UV/Vis light (Figure 2 c). In addition to the as-prepared $WO_3 \cdot H_2O$, NH_3 evolution was also tested over carbon modified commercial $WO_3 \cdot H_2O$ (HWO-com/C). The activity difference can be attributed to the different specific surface area of two $WO_3 \cdot H_2O$ supporters (Supporting Information, Figure S7). Above results indisputably indicate the indispensable roles of both carbon decoration and photoactive $WO_3 \cdot H_2O$ for efficient NH_3 evolution.
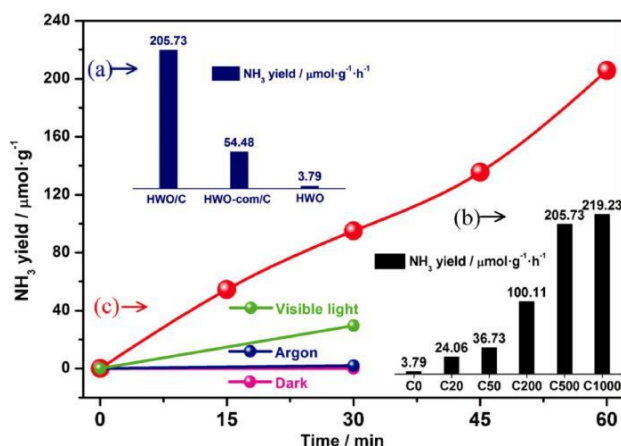
Figure 2. Photocatalytic N_2 fixation rate. (a) Photocatalytic N_2 fixation rates of different samples. (b) Photocatalytic N_2 fixation rates of HWO/C-X sam-ples. (c) Photocatalytic N_2 fixation rates of HWO/C500 with time under UV/Vis light (red), dark (pink), visible light (green) and argon atmosphere (blue), respectively.

Careful studies were conducted to explore the decisive role of carbon decoration in N_2 photoreduction. Raman spectrosco-py was firstly recorded to investigate the precise structure of the supported carbon. As shown in Figure 3 a, absorptions before 1000 cm^{-1} are ascribed to $WO_3 \cdot H_2O$, and the absorp-tions at 1600–1300 cm^{-1} belong to carbon. Specifically, the peak at 1580 cm^{-1} stems from the absorption of carbon with sp2 hybridization, and the peak at about 1345 cm^{-1} is ascribed to carbon with sp3 hybridization. The intensity ratio of the D to the G peak (ID/IG) is 0.807 and the high G band is ascribed to the graphitic clusters embedded in the amorphous matrix.[9] This point was further confirmed by X-ray photoelectron spec-troscopy (XPS), for which the C1s peak around 284.84 and 285.8 eV indicates the mixed sp2 and sp3 bonding (Supporting
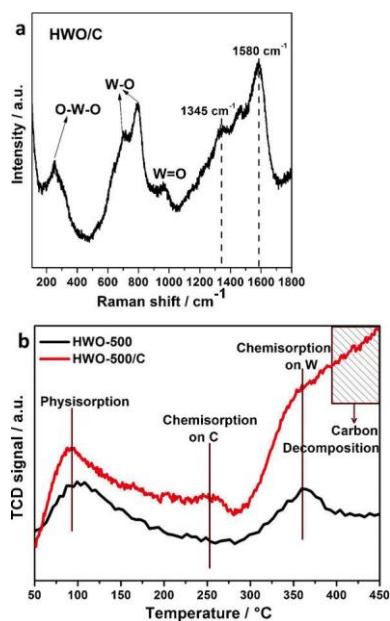
Figure 3. (a) Raman spectra of HWO/C. (b) N_2-TPD profiles of the as-prepared HWO-500 and HWO-500/C photocatalysts.

Information, Figure S9).[10] According to the literature, the N N triple bond can be evidently weakened at the unsaturated carbon, including the edge of the armchair graphite surface or the tip of a capped (5, 5) single-walled carbon nanotube.[11]   It is proposed that the sp2 bonded carbon in the hybridized structures is capable of exhibiting the reactive role toward the absorption and activation of N_2 molecular. Temperature-programmed desorption (TPD) investigations have been conducted to visualize the activation of N_2 on the surface of the HWO-500 and HWO-500/C since $WO_3 \cdot H_2O$ easily loses the crystallized water when the temperature is higher than 250 8C. As shown in Figure 3 b, except for the physical absorptions at approximately 100 8C, one peak at 350 8C and two peaks at 250 and 350 8C were observed for HWO-500 and HWO-500/C, respectively. The uplift of TCD signal after 350 8C of the HWO-500/C was attributed to the decomposition of carbon. Earlier work has established the electrochemical feasibility of NH_3 production cycles with tungsten.[12] This finding indicated the N_2 chemisorption on both W and C. Furthermore, the higher binding energy between W and N_2 was disadvantageous to the photocatalytic process and the weaker binding between C and N was favorable for the reduction.

In addition to the surface N_2 activation, photoinduced protonation with electron/proton transfer is another elementary step in N_2 reduction to NH_3. Due to its outstanding electron and proton conductivity, photoactive $WO_3 \cdot H_2O$ played an important role in this process. In photocatalysis, efficient photon-to-electron (PE) conversion is required for a high photon-to-product quantum yield. As indicated in Figure 4 a, under light irradiation the Nyquist plot of a   HWO electrode presented a much smaller semicircle in the high-frequency region compared to that in the dark, indicating greatly promoted charge-separation and transport in photoexcited HWO. The electron

transport can be further enhanced by carbon decoration, confirmed by the smaller semicircle of the Nyquist plot recorded over an HWO/C electrode (Figure 4 a). Another evidence of enhanced PE conversion within HWO/C was the much higher photocurrent density. As indicated in Figure 4 b and c, the current response reaches up to 20 mA for HWO/C, whereas it is about 2 mA for HWO. Interestingly, the transient current responses in the N_2-bubbled electrolyte were much smaller than that in the presence of Ar, indicating a certain kind of photoinduced electron consumption by N_2. Notably, for HWO/C the current reduction was nearly 80 %, whereas for HWO it was merely 15 %. Given the above discussion about N_2 dissociation on a carbon surface, the electrochemical measurements provide another convictive supplement to the TPD data for verifying the decisive role of carbon within the hybrid. Besides the electron generation and transport, sufficient proton supply is also pivotal for protonation. In order to verify this point, we controlled the amount of hydrate water within the HWO-C hybrid by calcining HWO at different temperatures in air before surface carbon decoration. As shown in the XRD pattern (Supporting Information, Figure S10), HWO was gradually transformed to WO_3 by calcination at 500 8C with the gradual loss of crystal water. As a result, the NH_3 evolution by N_2 reduction was greatly suppressed over partly dehydrated HWO/C, presenting rates of 194.9, 94.2 and 17.2 mmol $g^{@1}$ $h^{@1}$ when HWO was treated at 100, 300, and 500 8C, respectively. In order to understand the effect of surface area on the photoreactivity of calcined samples, the NH_3 evolution rates were normalized with surface areas (Figure 4 d, and Supporting Information Table S1). The k/BET of HWO-300/C (3.37) was close to that of HWO-100/C (3.13), however, the k/BET of HWO-500/C (1.16) reduced greatly. It was found that the existence of crystal water improved the efficiency of the reaction. $WO_3 \cdot H_2O$ was reported to be easily injected with protons and electrons.[13] These results suggest the necessity of unbroken crystalline structure of HWO for photoinduced protonation, probably due to the intrinsic proton conductivity. We further explored the source of protons in the final product NH_3. On one hand, after prolonged N_2 photofixation, neither performance reduction of NH_3 evolution nor decomposition of HWO into WO_3 was observed, indicating the retention of protons within HWO. On the other hand, O_2 evolution in the reaction system during N_2 photofixation was found to be nearly stoichiometric according to Equation (1). As evidence, the photocurrents of HWO-100/C and HWO-500/C were tested in the nonprotic electrolyte CH_3CN with different amounts of water (Supporting Information, Figure S11). The HWO-100/C exhibited greater decreases when 0.4 vol % water introducing and indicated N_2 reacted with the proton in the water and the HWO-100/C exhibited better conductivity of the proton.[14] Moreover, the CV of HWO/C in N_2 atmosphere was presented in Figure 5. The reduction potential was linearly correlated with the decease of pH. According to the following formula:[15] dEp/dpH =2.303 mRT/nF, in which m is the number of protons, n is the number of electrons, and m/n is calculated to be 3 for the reduction process. This indicated that the number of protons was triple that of the electrons involved in the electroreduction process, which proved the
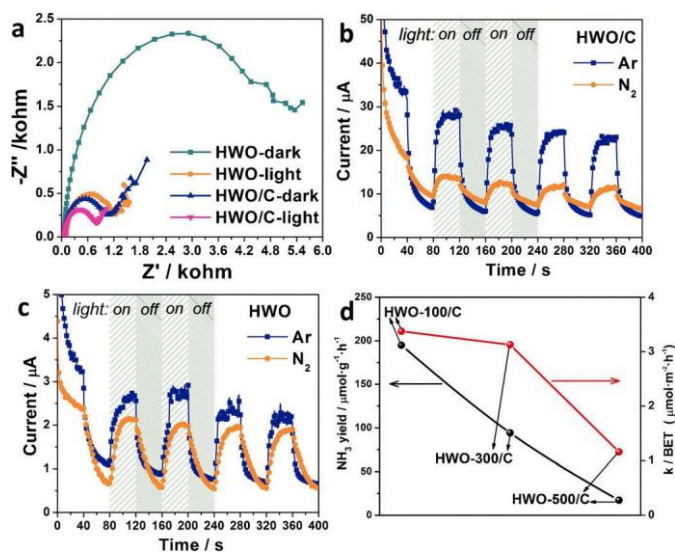
Figure 4. (a) Electrochemical impedance spectroscopy Nyquist plots with or without Xe lamp irradiation over HWO and HWO/C. Transient current - time curves over HWO/C (b) and HWO (c) electrodes in an Ar or N_2 atmosphere.

(d) Photocatalytic N_2 fixation rates and rates normalized with BET of HWO-Y/C (Y represents the different calcination temperatures).
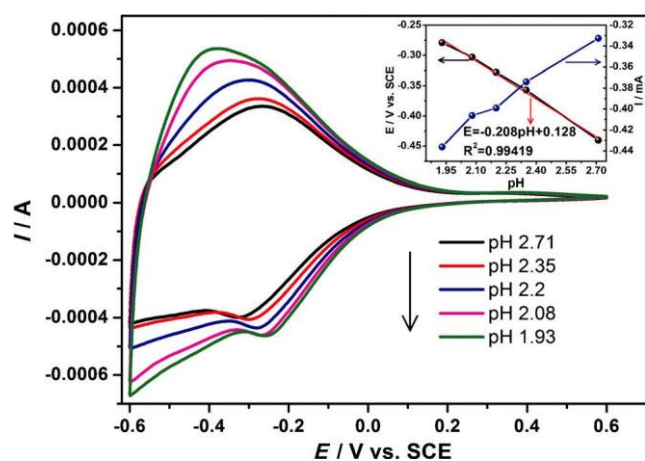
Figure 5. Cyclic voltammograms (CV) of HWO/C on glass carbon electrodes in the solutions with different pH values. Inset: the influence of pH on the reduction peak current and potential.

proton-coupled electron transfer. And during the NH_3 evolu-tion process, a little amount of N_2H_4 was detected in the system (Supporting Information, Figure S12). The success of the N_2 fixation on the HWO/C was attributed to the multistep delivery of successive self-excited electrons and water-derived protons to N_2. Thus the proposed transfer of proton and elec-tron in the process was as shown in Scheme S1 (Supporting In-formation). Based on above results, the original source of proton in photogenerated NH_3 should be water, but not the hydrate water within HWO. The HWO played indispensable role in the dissociation of H_2O to O_2 and proton and the con-ductivity of the proton. For detail, the O_2 evolution was more than NH_3 formation result of the dissolution of O_2 in water (Supporting Information, Figure S13). The reasons of the reduc-tion of NH_3 might be that the protons were transferred to compound H_2 and the O_2 oxidized the NH_3 in the closed system. The cycle experiment was achieved on the HWO/C (Supporting Information, Figure S14). Though the performance of the fresh catalyst was reduced after the first cycle, the NH_3 evolution rates (ca. 100 mmol $g^{@1}$ $h^{@1}$) turned to be stable from the second cycle (Supporting Information, Figures S15–S18).

$$2\,N_2 þ 6\,H_2O \rightarrow 4\,NH_3 þ 3\,O_2 \qquad\qquad ð1Þ$$

In addition to above carbon-HWO hybrids, we further exam-ined the universality of surface carbon modification for en-hancing N_2 photoreduction over other materials. Although these systems have not yet been optimized, the results in Fig-ure S19 (Supporting Information) revealed that photocatalytic NH_3 evolution over P25, anatase TiO_2 and BiOBr can be signifi-cantly enhanced by decoration small amounts of carbon on semiconductor surface, clearly indicating the universality of the carbon decoration strategy.

In summary, highly efficient N_2 photofixation to NH_3 was achieved over carbon-$WO_3 \cdot H_2O$ hybrids in pure water without any additives or cocatalysts. On one hand, carbon greatly en-hances the surface N_2 activation as well as the separation and transport of photogenerated charge carriers. On the other hand, photoactive $WO_3 \cdot H_2O$ with outstanding electron/proton conductivities guaranteed the supply of required electrons and protons for subsequent protonation. The universality of carbon modification for enhancing the N_2 reduction was further veri-fied over other materials. This carbon decoration strategy might guide the future design of efficient systems for solar-driven N_2 fixation.

Acknowledgements

[1] a) S. Giddey, S. P. S. Badwal, A. Kulkarni, Int. J. Hydrogen Energy 2013, 38, 14576 – 14594; b) M. E. Bluhm, M. G. Bradley, R. Butterick, U. Kusari, L. G. Sneddon, J. Am. Chem. Soc. 2006, 128, 7748 – 7749; c) J. W. Erisman, M. A. Sutton, J. Galloway, Z. Klimont, W. Winiwarter, Nat. Geosci. 2008, 1, 636 – 639.

[2] a) M. Steinberg, H. C. Cheng, Int. J. Hydrogen Energy 1989, 14, 797 – 820; b) S. Licht, B. Cui, B. Wang, F. F. Li, J. Lau, S. Liu, Science 2014, 345, 637 – 640.

[3] a) O. Rusina, A. Eremenko, G. Frank, H. P. Strunk, H. Kisch, Angew. Chem. Int. Ed. 2001, 40, 3993 – 3995; Angew. Chem. 2001, 113, 4115 – 4117; b) N. N. Rao, S. Dube, Manjubala, P. Natarajan, Appl. Catal. B 1994, 5, 33 – 42; c) G. N. Schrauzer, T. D. Guth, J. Am. Chem. Soc. 1977, 99, 7189 – 7193.

[4] a) Y. Nishibayashi, Inorg. Chem. 2015, 54, 9234 – 9247; b) C. Sivasankar, S. Baskaran, M. Tamizmani, K. Ramakrishna, J. Organomet. Chem. 2014, 752, 44 – 58.

[5] T. Kandemir, M. E. Schuster, A. Senyshyn, M. Behrens, R. Schlçgl, Angew. Chem. Int. Ed. 2013, 52, 12723 – 12726; Angew. Chem. 2013, 125, 12955 – 12959.

[6] A. Banerjee, B. D. Yuhas, E. A. Margulies, Y. Zhang, Y. Shim, M. R. Wasie-lewski, M. G. Kanatzidis, J. Am. Chem. Soc. 2015, 137, 2030 – 2034.

[7] a) H. Li, J. Shang, Z. Ai, L. Zhang, J. Am. Chem. Soc. 2015, 137, 6393 – 6399; b) G. Dong, W. Ho, C. Wang, J. Mater. Chem. A 2015, 3, 23435 – 23441.

[8] a) M. Seifollahi Bazarjani, M. Hojamberdiev, K. Morita, G. Q. Zhu, G. Cher-kashinin, C. Fasel, T. Herrmann, H. Breitzke, A. Gurlo, R. Riedel, J. Am. Chem. Soc. 2013, 135, 4467 – 4475; b) Z. Chen, Y. Peng, F. Liu, Z. Le, J. Zhu, G. Shen, D. Zhang, M. Wen, S. Xiao, C. P. Liu, Y. Lu, H. Li, Nano Lett. 2015, 15, 6802 – 6808.

[9] L. Zhang, X. Wei, Y. Lin, F. Wang, Carbon 2015, 94, 202 – 213.

[10] S. T. Jackson, R. G. Nuzzo, Appl. Surf. Sci. 1995, 90, 195 – 203.

[11] a) Y.-J. Xu, J.-Q. Li, Chem. Phys. Lett. 2005, 406, 249 – 253; b) M. D. Ganji, Nanotechnology 2008, 19, 025709.

[12] C. J. Pickett, J. Talarmin, Nature 1985, 317, 652 – 653.

[13] a) S. H. Baeck, K. S. Choi, T. F. Jaramillo, G. D. Stucky, E. W. McFarland, Adv. Mater. 2003, 15, 1269 – 1273; b) B. W. Faughnan, R. S. Crandall, M. A. Lampert, Appl. Phys. Lett. 1975, 27, 275 – 277.

[14] H. Li, J. Shang, J. Shi, K. Zhao, L. Zhang, Nanoscale 2016, 8, 1986 – 1993.

[15] E. Laviron, J. Electroanal. Chem. 1974, 52, 355 – 393.